

# Resolve Domain Conflicts for Generalizable Remote Physiological Measurement

Weiyu Sun  
weiyusun@smail.nju.edu.cn  
Nanjing University  
Nanjing, Jiangsu, China

Xinyu Zhang  
xinyuzhang@smail.nju.edu.cn  
Nanjing University  
Nanjing, Jiangsu, China

Hao Lu  
hlu585@connect.ust.hk  
The Hong Kong University of Science  
and Technology  
Guangzhou, Guangdong, China

Ying Chen\*  
yingchen@nju.edu.cn  
Nanjing University  
Nanjing, Jiangsu, China

Yun Ge  
geyun@nju.edu.cn  
Nanjing University  
Nanjing, Jiangsu, China

Xiaolin Huang  
xlhuang@nju.edu.cn  
Nanjing University  
Nanjing, Jiangsu, China

Jie Yuan  
yuanjie@nju.edu.cn  
Nanjing University  
Nanjing, Jiangsu, China

Yingcong Chen  
yingcong.ian.chen@gmail.com  
The Hong Kong University of Science  
and Technology  
Guangzhou, Guangdong, China

## ABSTRACT

Remote photoplethysmography (rPPG) technology has become increasingly popular due to its non-invasive monitoring of various physiological indicators, making it widely applicable in multimedia interaction, healthcare, and emotion analysis. Existing rPPG methods utilize multiple datasets for training to enhance the generalizability of models. However, they often overlook the underlying conflict issues across different datasets, such as (1) label conflict resulting from different phase delays between physiological signal labels and face videos at the instance level, and (2) attribute conflict stemming from distribution shifts caused by head movements, illumination changes, skin types, etc. To address this, we introduce the D<sub>O</sub>main-H<sub>A</sub>rm<sub>O</sub>nious framework (DOHA). Specifically, we first propose a harmonious phase strategy to eliminate uncertain phase delays and preserve the temporal variation of physiological signals. Next, we design a harmonious hyperplane optimization that reduces irrelevant attribute shifts and encourages the model's optimization towards a global solution that fits more valid scenarios. Our experiments demonstrate that DOHA significantly improves the performance of existing methods under multiple protocols. Our code is available at <https://github.com/SWY666/rPPG-DOHA>.

## CCS CONCEPTS

• Applied computing → Health informatics.

\*Corresponding authors

Permission to make digital or hard copies of all or part of this work for personal or classroom use is granted without fee provided that copies are not made or distributed for profit or commercial advantage and that copies bear this notice and the full citation on the first page. Copyrights for components of this work owned by others than the author(s) must be honored. Abstracting with credit is permitted. To copy otherwise, or republish, to post on servers or to redistribute to lists, requires prior specific permission and/or a fee. Request permissions from [permissions@acm.org](mailto:permissions@acm.org).

MM '23, October 29–November 3, 2023, Ottawa, ON, Canada

© 2023 Copyright held by the owner/author(s). Publication rights licensed to ACM.

ACM ISBN 979-8-4007-0108-5/23/10...\$15.00

<https://doi.org/10.1145/3581783.3612265>

## KEYWORDS

physiological signal estimation, rPPG, multimedia application

### ACM Reference Format:

Weiyu Sun, Xinyu Zhang, Hao Lu, Ying Chen, Yun Ge, Xiaolin Huang, Jie Yuan, and Yingcong Chen. 2023. Resolve Domain Conflicts for Generalizable Remote Physiological Measurement. In *Proceedings of the 31st ACM International Conference on Multimedia (MM '23)*, October 29–November 3, 2023, Ottawa, ON, Canada. ACM, New York, NY, USA, 11 pages. <https://doi.org/10.1145/3581783.3612265>

## 1 INTRODUCTION

With wide application in multimedia [24, 26–28], remote photoplethysmography (rPPG) can estimate various physiological indicators from facial video and further apply to fields such as human-computer interaction [1, 43], emotional computing [13, 37] and security authentication [19, 55, 57]. Unlike traditional physiological measurement techniques like photoplethysmography (PPG), which require physical contact [47], rPPG offers a more convenient and cost-effective solution. By analyzing chrominance variations [53] in facial videos, rPPG can extract the underlying physiological periodic signal known as the rPPG signal. This can be achieved effortlessly, even through a basic webcam. The rPPG signal carries information about the cardiac activity, which can be derived using established practices used for other signal types such as blood volume pulse (BVP) signals [59, 60]. The advantage of rPPG lies in its non-contact nature and the ability to obtain physiological information remotely. Despite the potential advantages of rPPG, the fragility of the rPPG signal poses challenges for traditional algorithm-based rPPG methods [7, 48, 52] when faced with demanding tasks, such as videos that suffer from illumination variation or head movement.

Recently, deep learning (DL) networks have emerged as effective tools for assisting rPPG signal extraction. With the accumulation of existing works [5, 10, 11, 16, 20, 22, 30, 32, 33, 40, 41, 46, 58, 60], DL-based rPPG methods have demonstrated significantly better performance than traditional methods [7, 17, 35, 48, 52] over various

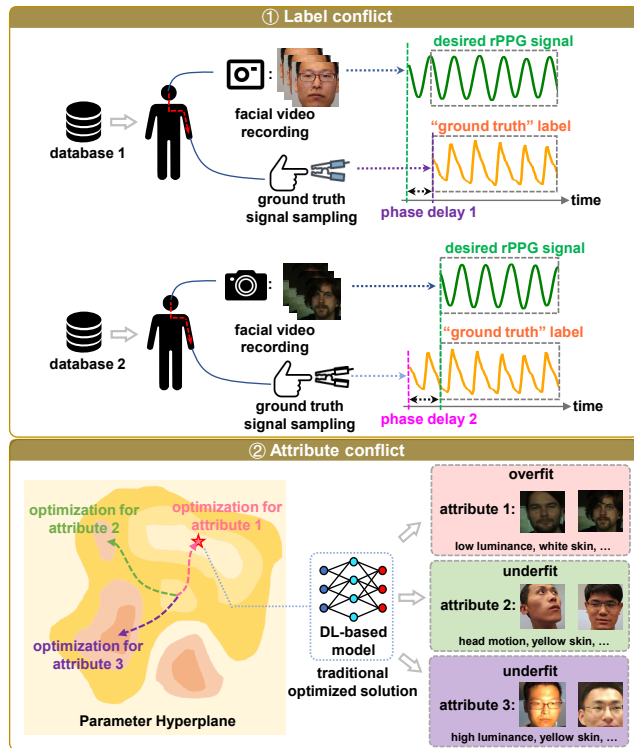


**Figure 1: Contradictory factors exist in rPPG model training.** ①: Label conflicts caused by different pulse transit times (red dashed line) and sampling equipment, which result in the chaotic phase delays between desired rPPG signals and “ground truth” signals among different databases. ②: Irrelevant attribute conflicts raised by diverse external noise (e.g., illumination, head motion). Such diversity and the predominance of the intensity over the rPPG signal make the optimization difficult to cover all involved domains.

intra-dataset [2, 31, 42] conditions. But in turn their performance against unseen scenarios is less impressive [23]. Therefore, for better practical performance, currently multiple datasets are used for network optimization [23] to improve the generalization of these deep learning models.

However, there are many obstacles preventing DL rPPG models from benefiting via multiple dataset training. These obstacles mainly derive from the domain conflicts between different databases. As shown in Fig. 1, we conclude these conflicts into two categories: label conflict and attribute conflict. The label conflict mainly refers to the phase delay differentials raised by different pulse transit times [11, 39] of subjects and different “ground truth” label sampling equipment. These phase delay differentials reduce the label stability, which can lead to pool learning efficiency for the DL rPPG model. The attribute conflict, on the other hand, is raised by the vulnerability of rPPG signal [48, 52] against external attributes (e.g., illumination, head motion, skin type) in facial videos. The rPPG signal is feeble (pixel level) [52], which makes the DL model easily dominated by the aforementioned external attributes (or domain-specific features). As a result, DL-based models tend to learn the relationship between different irrelevant attributes and different

label delays, which leads to the failure to learn a generalized physiological representation.

In this paper, we propose the D<sub>O</sub>main-H<sub>A</sub>rmonious framework (DOHA), which addresses both label conflict and attribute conflict for rPPG tasks. Specifically, we design a harmonious phase strategy (DOHA-HPS) that transfers the temporal physiological information into a self-similar representation (termed as self-similarity physiological map) to alleviate label conflicts. This strategy preserves the negative effects of elusive phase differentials. Then, we propose a harmonious hyperplane optimization (DOHA-HHO) to reduce domain shift overfitting. DOHA-HHO first identifies those out-of-distribution instances based on their gradient norms and then restricts their impacts, termed as global gradient harmony (DOHA-GGH). Next, we perform instance-wise gradient surgery (namely instance-wise gradient harmony, DOHA-IGH) to alleviate conflicting components for the remaining instances in the batch, thus letting the model focus on the common feature (i.e. rPPG signal) among instances. This novel optimization strategy can not only alleviate model attributes overfitting at the instance level but also seek domain-shared features at the global level. Our contributions are summarized below:

- We define the domain conflict problem of the rPPG task, which limits the generalization ability of the model when using multiple datasets simultaneously.
- We propose a harmonious phase strategy, which can eliminate the negative effects of uncertain phase delays with maximally preserving the temporal information of physiological signals.
- We propose a harmonious hyperplane optimization strategy, which can alleviate irrelevant attributes overfitting at both instance and global levels.
- We provide extensive experimental results to demonstrate the effectiveness of DOHA.

## 2 RELATED WORK

### 2.1 Remote Photoplethysmography Technique

Remote photoplethysmography (rPPG) is one of the techniques of remote physiological measurement. It estimates HR and other health indexes (e.g., heart rate variability (HRV)) via analyzing the chrominance change (termed as rPPG signal) from the facial video. Early traditional rPPG methods [7, 17, 35, 48, 52] rely on the pre-defined algorithm based on physiological prior knowledge. Recently, the competence of deep learning contributes to various remarkable DL-based rPPG methods [5, 20, 22, 32, 33, 41, 58–60]. These DL-based rPPG methods can be divided into two categories: end-to-end methods [5, 20, 41, 58–60] that take in original facial videos, and non-end-to-end methods [22, 23, 32, 33] that first transform facial videos into specialized spatial-temporal (ST) maps before analysis. Despite their promising results, label conflict remains a challenge for these methods, and existing solutions are either costly (e.g., manual calibration [58]) or limited in their usage scenarios (e.g., requiring manual preprocessing [32]).

### 2.2 Domain Generalization

The domain generalization (DG) technique has shown promise in addressing the domain conflict problem discussed in Section 1. DG techniques aim to enhance the model’s ability to handle domain

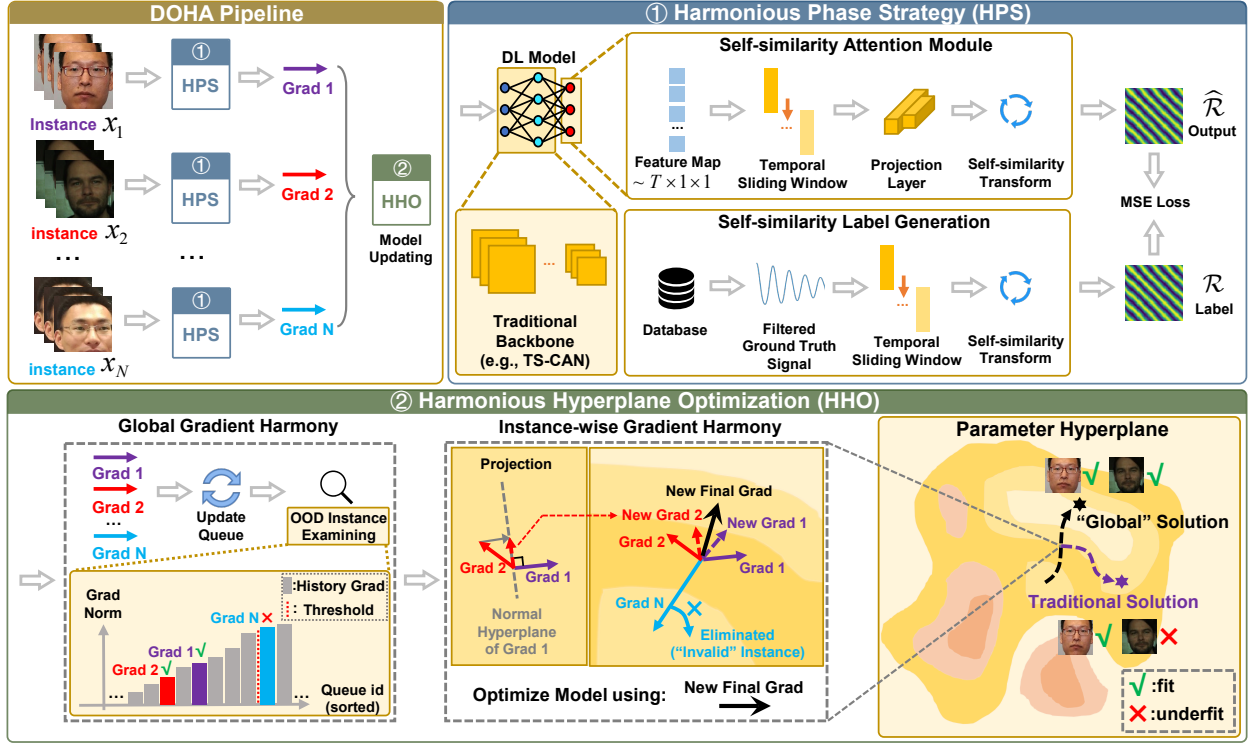


**Figure 2: An overview of our proposed method.** ① exhibits our harmonious phase strategy on ground truth signal and network output, respectively.  $\hat{\mathcal{R}}$  and  $\mathcal{R}$  present typical network output and label in the form of self-similarity physiological map. ②: a brief demonstration of Harmonious Hyperplane Optimization. Compared with the traditional optimization rule, it eliminates potential invalid instances (instance  $X_N$ ) and then de-conflicts remaining instances on the parameter hyperplane, so that the optimization can cover more attributes.

shifts, thereby improving its performance on unseen scenarios [9, 12, 25, 45, 49–51]. In the context of rPPG, various DG-related approaches have been explored [6, 23], including data augmentation methods [44], meta-learning [16], and representation learning [23]. However, these techniques often overlook or underestimate the negative effect of domain conflicts, resulting in insufficient improvement. The gradient surgery (GS) technique is a special form of the DG method that addresses potential conflicts during model training. It operates on backward gradients in the parameter hyperplane [25, 56], enabling effective optimization towards desired directions. This technique has been successfully applied in various training tasks to address conflicts between different tasks [56] or different domains [25]. However, the rPPG databases present unique complexities, as conflicts can arise at the instance level, and the difficulty of different instances can vary greatly and be elusive. This phenomenon poses challenges to the effectiveness of traditional gradient surgery [25], which relies on accurate domain labels (e.g., dataset classes). To address these challenges, we propose a specialized GS-based method called Harmonious Hyperplane Optimization for rPPG. This method offers a fine-grained and easy-to-implement approach to mitigate conflicts in the rPPG task.

### 3 METHODOLOGY

#### 3.1 Overall Framework

In this work, we propose the Domain-Harmonious framework (DOHA) to alleviate the aforementioned conflicts, as illustrated in

Fig. 2. First, for each instance in the batch, we collect the corresponding backward gradient via the harmonious phase strategy (DOHA-HPS, Fig. 2 ①). DOHA-HPS transforms the ground truth signal and model output into the self-similarity space, represented by  $\mathcal{R}$  and  $\hat{\mathcal{R}}$  respectively, to neutralize label conflicts. Next, we perform harmonious hyperplane optimization (DOHA-HHO, Fig. 2 ②) on the collected gradients. It consists of two parts: (1) Global gradient harmony (DOHA-GGH), which identifies and excludes the disharmonious instances that are not suitable for the overall optimization process. (2) Instance-wise gradient harmony (DOHA-IGH), which mitigates the conflicting portions among the remaining instances, preventing the model from overfitting on irrelevant attributes and underfitting on others.

#### 3.2 Harmonious Phase Strategy

**Motivation.** Phase delay differentials in rPPG databases are common, unavoidable, and elusive. These differentials arise from two main factors: (1) variations in the “ground truth” signal sampling equipment, where each device introduces different delays due to circuit design, and (2) pulse transit time (PTT) [11, 39], which represents the time it takes for the physiological signal to transit through the subject’s body (indicated by the red arrow in Fig. 1). The former factor leads to conflicts in labels across datasets, while the latter can cause conflicts at the instance level. These conflicts cannot be eliminated due to the inherent physiological nature and limitations of the techniques used. Although these conflicts can be observed

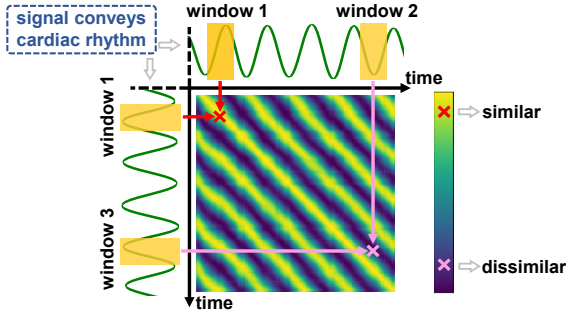


Figure 3: A typical self-similarity physiological map, where a higher value (bright) indicates that the temporal messages between two windows are similar, and vice versa. The “signal” can be a ground truth wave (e.g., BVP signal), or the predicted signal of the rPPG model.

in instances that can be analyzed by traditional rPPG methods (e.g., GREEN<sup>1</sup>), existing rPPG methods [7, 48, 52] have poor resistance against external noise (such as head motion), resulting in only a small fraction of instances being suitable for such analysis. Consequently, many valuable instances would be discarded, leading to both labor-intensive efforts and reduced data utilization. Therefore, there is a need for a cost-effective and efficient approach to address label conflicts.

**Self-similarity physiological map.** To this end, we propose the Harmonious Phase Strategy (DOHA-HPS) that provides an informative and stable label representation. DOHA-HPS leverages the concept of temporal self-similarity to mitigate the effects of phase delay while preserving important temporal physiological information. Specifically, we first divide the “ground truth” signal into different time windows using a sliding window and calculate the similarity (e.g., cosine similarity) among windows to form a matrix  $\mathcal{R}$ , as shown in Fig. 3<sup>2</sup>. Each element  $\mathcal{R}_{ij}$  indicates the similarity between the  $i_{th}$  and  $j_{th}$  temporal windows. As each element in  $\mathcal{R}$  depends only on the temporal distance between two windows and the cardiac period, the impact of delay differential is thus minimized.

**Self-similarity attention module.** Similarly, we can generate an output  $\hat{\mathcal{R}}$  at the end of the rPPG model, such as the BVP signal estimation head [23], as shown in Fig. 2 ①. And to better analyze temporal information, we insert a projection layer (e.g., linear layer) between temporal windows and self-similarity transform. As a result, both  $\mathcal{R}$  and  $\hat{\mathcal{R}}$  contain aligned temporal information and are derived from the subject’s cardiac activity. Therefore, we can define loss functions based on the similarity between  $\mathcal{R}$  and  $\hat{\mathcal{R}}$  to optimize the model. For sure, many potential loss function designs can be explored, and here we provide a typical loss item (i.e. Mean Squared Error (MSE) loss) for optimization, as shown in eq. (1).

$$\mathcal{L}_m = \frac{1}{N^2} \sum_{i=0}^{N-1} \sum_{j=0}^{N-1} (\mathcal{R}_{ij} - \hat{\mathcal{R}}_{ij})^2 \quad (1)$$

where  $N$  is the size of self-similarity physiological map  $\mathcal{R}$  and  $\hat{\mathcal{R}}$ .

<sup>1</sup>Traditional methods estimate the rPPG signal directly from the input video, instead of the sampling equipment, thus providing a reliable reference for delay detection. Readers can refer to the Appendix. D for more details.

<sup>2</sup>Detailed generation for  $\mathcal{R}$  and  $\hat{\mathcal{R}}$  can refer to Appendix C and algorithm 3.

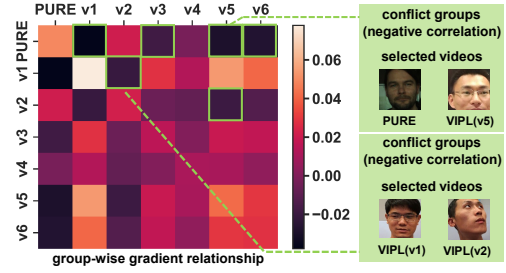


Figure 4: The gradient of baseline [20] has conflicts among both intra- and inter-dataset. For example, the average gradient of VIPL (subset v1-v6) [31] and PURE [42] prominently present the negative cosine similarity.

**Cardiac information inversion.** In the network output  $\hat{\mathcal{R}}_{N \times N}$ , the elements belonging to the set  $\{\hat{\mathcal{R}}_{ij} | i - j = t_m\}$  describe the relationship between two windows with a temporal distance of  $t_m$  ( $t_m \in [0, N - 1]$ ). By collecting element sets that belong to different  $t_m$  in  $\hat{\mathcal{R}}$ , we thus obtain an autocorrelation sequence  $Seq$  of the desired rPPG signal, from which we can extract physiological messages such as the heart rate ( $HR$ ). The detailed algorithm is depicted in Algorithm 1, where  $\mathcal{F}(\cdot)$  is a band-pass filter with a range of  $[0.7, 3.5]Hz$ , and  $\mathcal{D}(\cdot)$  analyzes peak distance<sup>3</sup> to determine the frequency (related with heart rate) of  $Seq$ . Noteworthy, more robust and effective methods for extracting information from  $\hat{\mathcal{R}}$  can be explored, such as non-end-to-end methods [32, 40] or two-dimensional spectrum analysis, which we leave for future research.

---

#### Algorithm 1 Cardiac Information Inversion

---

- 1: **Input:** network output  $\hat{\mathcal{R}}_{N \times N}$ , output size  $N$ , band-pass filter  $\mathcal{F}(\cdot)$ , peak detection algorithm  $\mathcal{D}(\cdot)$ .
  - 2: initialize autocorrelation sequence  $Seq: \{\}$
  - 3:  $Seq[t_m] \leftarrow \{\hat{\mathcal{R}}_{ij} | i - j = t_m\}, \forall t_m \in [0, N - 1]$
  - 4:  $Seq[t_m] \leftarrow mean(Seq[t_m])$
  - 5:  $HR = \mathcal{D}(\mathcal{F}(Seq))$
  - 6: **Output:** heart rate  $HR$
- 

### 3.3 Harmonious Hyperplane Optimization

**Motivation.** Compared to external factors (e.g., illumination variation and head motion), the rPPG signal is very feeble, leading the learning of the rPPG model vulnerable to irrelevant attribute conflicts. To verify this, we examine the relationship (i.e. cosine similarity) of the backward gradients among instances from PURE and VIPL (task v1-v6<sup>4</sup>) databases on a DL-based model (TS-CAN [20]) pre-trained using these databases, as shown in Fig. 4. According to the illustration, we observe the prominent negative correlation between PURE and VIPL (e.g., VIPL v1, VIPL v5), and such disharmony persists even within the VIPL dataset (e.g., v1 and v2). Conceivably, these conflicts can be more prevalent and difficult to identify outside controlled laboratory environments.

**Instance-wise gradient harmony.** The observed conflicts in gradients suggest that the model training is hindered by irrelevant attributes and fails to capture the inherent pattern extraction of

<sup>3</sup>Such as the function “signal.find\_peaks” in “scipy” package.

<sup>4</sup>The detailed information of task v1-v6 of VIPL database can refer to the Appendix A.



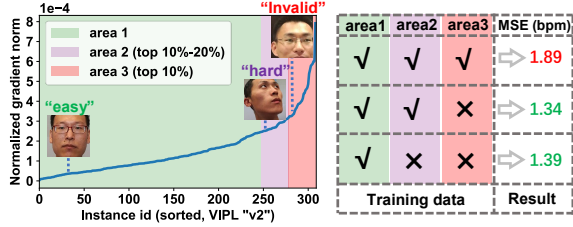


**Figure 5: Potential invalid instances (i.e., those with larger gradient norms, area 3) can be disharmonious with others, leading to worse performance of the rPPG model. The involved training instances are collected from task v2 in VIPL [31] database, the testing sets are PURE [42] and UBFC [2].**

rPPG. To mitigate this, we propose to harmonize the training process by resolving these conflicts in the parameter hyperplane, which has been shown to be effective in existing works [25, 56]. However, as observed in Fig. 4, these conflicts are pervasive throughout the dataset, rendering traditional domain labels (e.g., dataset classes) too coarse-grained to represent the clusters of the same attribute [23]. Therefore, we select to perform gradient surgery at the instance level, i.e., view each instance as a single cluster. Specifically, before optimizing the model, we first calculate the backward gradient  $\mathcal{G}_i$  for each instance  $x_i$  ( $i \in [0, N - 1]$ ) in the batch of instances  $x_0, x_1, \dots, x_{N-1}$ . Then, we neutralize the conflicting portions of the collected backward gradients by obeying the following rule: if two gradients  $\mathcal{G}_i$  and  $\mathcal{G}_j$  are negatively related (i.e., their cosine similarity is negative), then the gradient of each instance is projected onto the normal hyperplane of the gradient of the other instance, as shown in Equation. (2).

$$\mathcal{G}_i = \mathcal{G}_i - \frac{\mathcal{G}_i \cdot \mathcal{G}_j}{\|\mathcal{G}_j\|^2} \mathcal{G}_j \quad (2)$$

where  $\|\mathcal{G}_j\|$  represent the norm of  $\mathcal{G}_j$ . This operation restricts the conflicting portions of the gradients between two instances while preserving the common parts. And we iteratively apply equation (2) to each gradient pair  $\mathcal{G}_i$  and  $\mathcal{G}_j$  ( $i, j \in [0, N - 1], i \neq j$ ), as outlined in Algorithm 2 (lines 4-9). By doing so, we thus filter out irrelevant external attributes within the training batch and retain the common information (rPPG), which allows the overall optimization direction to cover as many instances in the batch as possible. Consequently, the deep learning model can learn a generalized way of extracting rPPG signals under different training domains.

**Global gradient harmony.** The rPPG signal is susceptible to external noise, and in extreme cases, certain instances may be considered invalid due to the overwhelming presence of noise. This phenomenon results in a wide range of difficulty levels among training instances, which is not conducive to the model learning [4, 18]. The presence of these invalid instances poses a challenge for our harmonious hyperplane optimization, as they may introduce the distorted normal hyperplanes during the gradient projection step (eq. (2)), thus compromising the integrity of the harmonized gradient. As illustrated in Fig. 5, restricting these potential invalid instances (i.e., samples with abnormal gradient norms [18]) can significantly upgrade the performance of the rPPG method [20].

In light of this, we aim to mitigate the negative effects of these invalid instances by sifting out the out-of-distribution (OOD) instances during the optimization, as shown in Algorithm 2 (line 3, 9).

Specifically, we introduce a global queue *Queue* with max length  $L$  (150 by default) to record the backward gradients of previous instances. Each time before stepping the optimization, we compare the current backward gradients  $\mathcal{G}_0, \mathcal{G}_1, \dots, \mathcal{G}_{N-1}$  with the *Queue*. If any instance (for example,  $\mathcal{G}_i$ ) in the batch exhibits a significantly larger gradient (larger than 95% gradients, i.e.,  $Top_{(5\%)}(Queue)$  over the norm in *Queue*), we temporally remove the instance (i.e., set it to zero vector) from the current turn of optimization. Noteworthy, the removed instance will not be permanently discarded. With the rPPG model continuing to learn over time, it can gradually identify and utilize these previous invalid instances to handle high-difficulty tasks. Thus we can globally select the most suitable instances to ensure the progressive training of the rPPG model.

Based on discussions above, we conclude our harmonious hyperplane optimization in Algorithm 2, where  $\mathbb{I}(\cdot)$  is the indicator function. Noteworthy, the loss function  $\mathcal{L}(\cdot, \cdot)$  in Algorithm 2 can vary depending on the training strategy. For the harmonious phase strategy,  $\mathcal{L}(\cdot, \cdot)$  can be eq. (1); for traditional wave-based training strategies [5, 20, 58],  $\mathcal{L}(\cdot, \cdot)$  can be negative Pearson loss [59], etc.

#### Algorithm 2 Harmonious Hyperplane Optimization (DOHA-HHO)

- 1: **Input:** DL-based model  $f_\theta(\cdot) : \mathcal{X} \rightarrow \mathcal{Y}$ , batch size  $N$ , batch of input data  $\{x_0, x_1, \dots, x_{N-1}\}$ , batch of ground truth label  $\{y_0, y_1, \dots, y_{N-1}\}$ , loss function  $\mathcal{L}(\cdot, \cdot)$ , threshold  $T$ , gradient record list *Queue*.
- 2:  $\mathcal{G}_i \leftarrow \nabla_{\theta} \mathcal{L}(f_\theta(x_i), y_i), \forall i \in [0, N - 1]$
- 3:  $\mathcal{G}_i^{GS} \leftarrow \mathbb{I}(\|\mathcal{G}_i\|_2 < Top_{(T\%)}(Queue))(\mathcal{G}_i), \forall i \in [0, N - 1]$
- 4: **for**  $i \in [0, N - 1]$  **do**
- 5:     **for**  $j \sim [0, N - 1] \setminus i$  in random order **do**
- 6:         **if**  $\mathcal{G}_i^{GS} \cdot \mathcal{G}_j < 0$  **then**
- 7:             Conduct  $\mathcal{G}_i^{GS} = \mathcal{G}_i^{GS} - \frac{\mathcal{G}_i^{GS} \cdot \mathcal{G}_j}{\|\mathcal{G}_j\|^2} \mathcal{G}_j$
- 8: Update  $f_\theta(\cdot)$  via  $\Delta\theta = \sum_i \mathcal{G}_i^{GS} / N$
- 9: Update *Queue* with  $\|\mathcal{G}_0\|_2, \|\mathcal{G}_1\|_2, \dots, \|\mathcal{G}_{N-1}\|_2$

## 4 EXPERIMENTS

### 4.1 Datasets

**VIPL-HR** [31] is a large-scale dataset for remote physiological measurement, it contains different tasks covering different ambient light conditions and motion intensities on 107 subjects recorded by 4 different devices. **UBFC** [2] contains 42 videos recorded from 42 subjects respectively. **PURE** [42] contains facial videos recorded from 10 subjects, each subject participates in 6 different tasks (sitting still, talking, four variations of head movement). Like [23], when collecting training instances, we align the frame rate to 30 fps by interpolation.

### 4.2 Implementation Details

**Training Details.** All experiments can be conducted on a single GeForce RTX 3090 graphic card. When processing facial videos, we utilize the “mmod face detector” [14] from the “dlib” python package to detect human faces. We then resize each detected region to a shape of  $[151 \times 151]$ . For data augmentation, we apply RandomCrop by randomly selecting a  $[131 \times 131]$ <sup>5</sup> region from the original

<sup>5</sup>We slightly adjust the entrance of involved network pipeline [5, 20, 58] to fit the input size, the detailed adjustment refers to Appendix B.

**Table 1: Heart rate (HR) estimation results over three simulated unseen scenarios under multiple dataset protocol, <sup>+</sup> indicates applying this method (on the Baseline [20] by default). The unit of HR is bpm (i.e., beat per minute).**

Method	VIPL			UBFC			PURE		
	MAE↓	RMSE↓	r↑	MAE↓	RMSE↓	r↑	MAE↓	RMSE↓	r↑
GREEN [48]	16.37	21.90	0.27	7.68	11.15	0.55	3.12	7.36	0.81
CHROM [7]	11.28	15.12	0.54	4.88	8.71	0.83	2.57	6.85	0.84
POS [52]	12.94	18.73	0.38	4.33	8.44	0.85	2.77	4.51	0.91
PhysNet [58]	10.43	16.03	0.44	2.03	3.12	0.94	2.54	4.33	0.92
Deepphys [5]	12.35	15.48	0.43	1.78	2.96	0.95	4.01	6.69	0.85
TS-CAN [20]	12.12	14.12	0.48	1.58	2.71	0.96	3.75	6.13	0.88
SAM <sup>+</sup> [8]	12.01	13.78	0.47	1.67	3.35	0.95	3.59	6.01	0.88
Domain GS <sup>+</sup> [25]	11.47	14.11	0.48	1.59	2.70	0.96	3.61	6.21	0.87
NEST[23]	11.01	14.33	0.49	1.54	3.01	0.97	2.93	4.13	0.90
Baseline [20]	12.12	14.12	0.48	1.58	2.71	0.96	3.75	6.13	0.88
DOHA <sup>+</sup> (w/o HPS)	10.73	13.71	0.53	1.53	2.81	0.97	1.78	2.96	0.91
DOHA <sup>+</sup> (w/o GGH)	7.46	12.09	0.61	1.76	2.95	0.96	1.25	2.31	0.95
DOHA <sup>+</sup> (w/o IGH)	7.38	11.77	0.62	1.46	1.83	<b>0.98</b>	1.03	1.79	0.98
DOHA <sup>+</sup>	<b>6.98</b>	<b>10.95</b>	<b>0.67</b>	<b>1.41</b>	<b>1.56</b>	<b>0.98</b>	<b>0.95</b>	<b>1.58</b>	<b>0.99</b>

[151 × 151] frame for each video. We eliminated the temporal padding in the baseline [20] to ensure the quality of the information on collected temporal windows. The training video clip length is set to 75, the default batch size is 4, and the total training epoch is 20. We employ the “adam” optimizer [61] with a cosine learning rate (lr) scheduler [21] (initial lr 5e-4, min lr 1e-6) to train DL models. During testing, the input video clip length is set to 300, which follows the same protocol [32, 60]. The default sifting threshold  $T$  in DOHA-GGH is set as 5, and the length of the *Queue* is 150. Before generating the self-similarity physiological map shown in Fig. 3, we first filter the ground truth wave (using a band-pass filter with [0.7, 3.5] Hz). We use the spatially averaged intermediate output  $x_{[T \times 1 \times 1]}$  of the last hidden layer in the DL model [5, 20, 58] to generate the output self-similarity physiological map  $\hat{R}$ . The default sliding window length  $L_w$  is set to 17. We use equation (1) as the loss function  $\mathcal{L}(\cdot, \cdot)$  to optimize the DL model with DOHA-HPS and follow the original traditional loss strategies of [5, 20, 32, 58] when training without DOHA-HPS.

**Performance Metrics.** We focus on the performance of heart rate (HR), heart rate variability (HRV), and respiration frequency (RF) estimations. Following previous works [22, 23, 32, 60], we adopt mean absolute error (MAE), root mean square error (RMSE), and Pearson correlation coefficient ( $r$ ) for evaluation.

### 4.3 Improvement on Multiple Dataset Training

**4.3.1 Improvement on HR Estimation.** We evaluated the HR estimation performance on unseen scenarios with three datasets: VIPL [31], PURE [42], and UBFC [2]. To simulate the unseen scenarios, we train the model on two datasets and then test it on the remaining dataset. We first compare DOHA against three traditional rPPG methods (GREEN [48], CHROM [7], and POS [52]) using the pyVHR package [3]. Then we re-implement three classical rPPG DL methods, i.e., DeepPhys [5], PhysNet [58], and TS-CAN [20]. As reported in [23], TS-CAN does not perform well against domain shift, so we use it as the baseline to evaluate the improvement of DOHA. Finally, we compare our method against three domain generalization (DG) methods, including SAM [8], DomainGS [25] and NEST [23].

**Table 2: Universality verification of DOHA on other widely-used rPPG methods. <sup>+</sup> means adopting DOHA on this method.**

Method	VIPL		
	MAE↓	RMSE↓	r↑
RhythmNet[32]	8.97	12.16	0.49
RhythmNet <sup>+</sup>	<b>7.75</b>	<b>10.97</b>	<b>0.63</b>
Deepphys[5]	12.35	15.48	0.43
Deepphys <sup>+</sup>	<b>7.48</b>	<b>11.04</b>	<b>0.61</b>
PhysNet[58]	10.43	16.03	0.44
PhysNet <sup>+</sup>	<b>7.33</b>	<b>12.25</b>	<b>0.62</b>

**The performance of traditional methods.** Tab. 1 shows that traditional methods can retain acceptable performance under simple scenarios like UBFC and PURE, but their performance significantly deteriorates in more challenging scenarios such as VIPL [31]. This suggests that these traditional methods that rely on static prior knowledge [52] may not be competent for handling complex tasks and thus are vulnerable to external factors such as head motion and illumination variation.

**The performance of DL-based rPPG methods.** As shown in Tab. 1, the involved DL methods, i.e., PhysNet [58], DeepPhys [5] and TS-CAN [20], exhibit merely comparable performance to traditional methods like POS [52] when facing all three unseen scenarios. Such result suggests that the baseline [20] has difficulty in learning generalized knowledge to analyze the rPPG signal under the traditional training setting (i.e. following the loss function [20] of the baseline), and this drawback is amplified under the multiple dataset training scenario where the domain conflicts within the training database are more severe.

**The performance of DG methods.** According to Tab. 1, none of the three domain generalization (DG) methods (i.e. SAM [8], Domain GS [25], and NEST [23]) show significant performance improvement over the baseline method [20]. We argue that this is due to their limited ability to address the underlying domain conflicts present in the training datasets. SAM’s approach [8] of achieving a smooth loss surface may lead to a sub-optimal solution that only

**Table 3: The improvement of DOHA over HRV and RF estimation, <sup>+</sup> indicates adopting this method to the Baseline [20].**

Target	Method	LF-(u.n)			HF-(u.n)			LF/HF			RF(Hz)		
		std↓	RMSE↓	r↑	std↓	RMSE↓	r↑	std↓	RMSE↓	r↑	std↓	RMSE↓	r↑
UBFC	GREEN [48]	0.246	0.305	0.1849	0.246	0.305	0.1849	1.094	1.275	0.1085	0.090	0.091	0.005
	CHROM [7]	0.226	0.292	0.317	0.226	0.292	0.317	1.020	1.120	0.275	0.084	0.085	0.079
	POS [52]	0.234	0.299	0.250	0.234	0.299	0.250	1.010	1.228	0.253	0.084	0.086	0.046
	Baseline [20]	0.216	0.259	0.396	0.216	0.259	0.396	1.014	1.186	0.403	0.087	0.087	0.047
	DOHA <sup>+</sup>	<b>0.212</b>	<b>0.258</b>	<b>0.429</b>	<b>0.212</b>	<b>0.258</b>	<b>0.429</b>	<b>1.007</b>	<b>1.178</b>	<b>0.418</b>	<b>0.083</b>	<b>0.083</b>	<b>0.101</b>
PURE	GREEN [48]	0.279	0.314	0.061	0.279	0.314	0.061	1.128	1.286	0.0848	0.084	0.085	-0.001
	CHROM [7]	0.245	0.305	0.172	0.245	0.305	0.172	1.086	1.287	0.115	0.091	0.093	0.004
	POS [52]	0.272	0.298	0.008	0.272	0.298	0.008	1.002	1.107	0.052	0.086	0.087	-0.021
	Baseline [20]	0.237	0.266	0.288	0.237	0.266	0.288	1.009	1.110	0.279	0.084	0.086	0.003
	DOHA <sup>+</sup>	<b>0.236</b>	<b>0.259</b>	<b>0.307</b>	<b>0.236</b>	<b>0.259</b>	<b>0.307</b>	<b>0.951</b>	<b>1.041</b>	<b>0.354</b>	<b>0.082</b>	<b>0.083</b>	<b>0.099</b>

**Table 4: HR estimation results over two unseen domains (VIPL and PURE), the training dataset is UBFC [2].**

Method	VIPL			PURE		
	MAE↓	RMSE↓	r↑	MAE↓	RMSE↓	r↑
GREEN[48]	16.37	21.90	0.27	3.12	7.36	0.81
CHROM[7]	11.28	15.12	0.54	2.57	6.85	0.84
POS[52]	12.94	18.73	0.38	2.77	4.51	0.91
Baseline[20]	12.21	19.89	0.44	2.67	7.63	0.80
DOHA <sup>+</sup>	<b>7.68</b>	<b>12.69</b>	<b>0.60</b>	<b>1.03</b>	<b>1.39</b>	<b>0.97</b>

covers certain parts of the training scenarios. The domain conflicts in rPPG databases are more complicated, which may exceed the capabilities of SAM to address effectively. Domain-based Gradient Surgery [25], which relies on coarse-grained domain labels, may not accurately capture the complex domain differences in rPPG databases, making it challenging to neutralize the domain conflicts thoroughly. Although NEST [23] performs better than the other two DG methods, it still does not fully address the label conflicts, which limits its further improvement.

**The performance of DOHA-HPS.** As demonstrated in Tab. 1, adopting our harmonious phase strategy can lead to a substantial improvement in performance for the baseline method [20]. This suggests that the harmonious phase strategy can provide a more appropriate label representation that assists the baseline to learn domain-invariant knowledge [9, 15, 34, 45]. By mitigating the phase delay differentials and focusing on the intrinsic relationship within the physiological signal, the new label representation thus serves as a better guide for the model, enabling it to achieve more generalized performance even in unseen scenarios.

**The performance of DOHA-HHO.** In Tab. 1, we observe that the harmonious hyperplane optimization improves the performance of the baseline method [20], both with and without the harmonious phase strategy. This result indicates that our DOHA-HHO can effectively address the attribute conflicts among rPPG datasets. As analyzed, the irrelevant attribute conflicts among instances exist in a fine-grained way, where the instance-wise gradient surgery can effectively cover and mitigate them. Moreover, the global gradient harmony helps maintain a balanced overall training data difficulty, thus preventing the model from being excessively influenced by instances that may lead to learning irrelevant attributes.

**4.3.2 Improvement on HRV and RF.** Following [23, 36, 60], we conduct experiments to examine the effect of DOHA-HHO on HRV (LF, HF, and LF/HF) and RF estimation using the PURE [42] and

**Table 5: DOHA can enhance the performance of baseline [20] to the level of existing state-of-the-art rPPG methods (i.e., PhysFormer[60], RhythmNet[32]) on VIPL dataset.**

Method	VIPL		
	MAE↓	RMSE↓	r↑
CHROM [7]	11.28	15.12	0.54
POS [52]	12.94	18.73	0.38
RhythmNet [32]	5.30	8.14	0.76
TS-CAN [20]	8.08	14.83	0.63
Physformer [60]	4.97	7.79	0.78
Dual-GAN [22]	4.93	7.68	0.81
Baseline [20]	8.08	14.83	0.63
DOHA+ (w/o HPS)	7.07	11.17	0.65
DOHA+ (w HPS)	5.01	8.49	0.78
DOHA+	<b>4.87</b>	<b>7.64</b>	<b>0.83</b>

UBFC [42] datasets. Likely, we train the model on one dataset and then test it on another to simulate the unseen scenario. As shown in Tab. 3, DOHA provides a more dominant performance for the baseline method [20], which indicates that our methodology not only extracts periodic features but also maximally preserves the temporal physiological information.

**4.3.3 Universality Verification.** DOHA is plug-and-play, making it able to take effect for both end-to-end methods [5, 58] and hand-manual (i.e. non end-to-end) methods [32]. To prove this, we train these models [5, 32, 58] on UBFC, PURE, and BUAA [54] and test the performance of DOHA on VIPL. As shown in Tab. 2, DOHA consistently improves the performance of all DL-based models. This is because, in DOHA, the harmonious hyperplane optimization introduces constraints to the gradient, which is a fundamental component of the DL training process. Additionally, the harmonious representation strategy can provide a more stable and universal physiological representation for these methods. These properties allow DOHA to take effect in various rPPG training scenarios.

## 4.4 Improvement on Single Dataset Training

**Single-Source Domain Generalization.** Under the worst case, only a single database is available for rPPG model training, which is termed as Single-Source domain generalization [23]. To verify the effect of DOHA under this situation, we conduct the experiment by training the baseline [20] on UBFC and then test its performance on PURE and VIPL. The results are shown in Tab. 4.

**Intra-Dataset Testing.** Following the experimental setup of [22, 32, 60], we conduct experiments to verify the effect of DOHA under

**Table 6: The impact of the projection layer in DOHA-HPS, where the “Identity” equals removing the projection layer.**

Projection Layer	Structure	VIPL		
		MAE↓	RMSE↓	r↑
Identity	-	7.82	13.19	0.57
Linear Layer	[88×88]	6.98	<b>10.95</b>	0.67
	[88×352]	<b>6.94</b>	11.65	<b>0.69</b>
BottleNeck	[88×88, 88×352, 88×88]	7.56	12.67	0.60

the intra-dataset scenario using a 5-fold subject exclusive cross-validation protocol on the VIPL dataset [31]. The baseline is TS-CAN [20]. The performance of DOHA and other state-of-the-art rPPG methods [22, 60] are presented in Tab. 5.

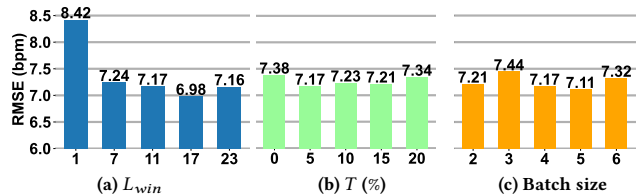
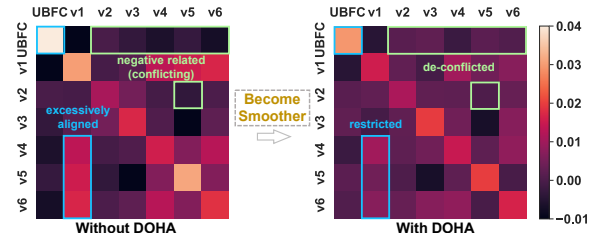
**Analysis.** According to the results, DOHA improves the performance of the baseline [20] under both two single dataset training scenarios. This confirms our assumption that the domain conflict phenomenon can also be pervasive within the single rPPG database [31]. In addition, the performance improvement by harmonious phase strategy (in Tab. 5) emphasizes that the information encoded in the self-similarity physiological map can effectively enhance the model’s learning of inherent facial cardiac feature analysis.

#### 4.5 Further Discussion

**The impact of  $L_{win}$ .** In DOHA-HPS, the sliding window length  $L_{win}$  determines the temporal perception to the physiological signal. We conduct an ablation study to seek the optimal  $L_{win}$ . As depicted in Fig. 6 (a), we observed that generally a longer sight (i.e., larger  $L_{win}$ ) results in improved performance. This phenomenon can be attributed to the fact that a longer sight allows the model to analyze the temporal information with more temporal context, thus enhancing its ability to resist burst noise (e.g., sudden, fierce subject’s movement). However, a longer  $L_{win}$  also introduces more temporal consumption, which can have a negative impact and needs to be carefully considered.

**The impact of  $T$ .** In DOHA-GGH, threshold  $T$  balances the global difficulty of participating instances. As shown in Fig. 5 and 6 (b), slightly restricting those out-of-distribution instances can properly enhance the training effect, which matches the experimental results in other fields [4, 18]. Noteworthy, for databases with higher diversity in difficulty levels (e.g., VIPL v2), the effect of DOHA-GGH can be more pronounced. But larger  $T$  reduces the utilization of the dataset, which may hurt the generalization of model [38].

**Discussion on the projection layer.** In the self-similarity attention module, a projection layer is added to interpret the feature of temporal windows. We verify the effect of different projection layers (i.e., identity, single linear layer, and bottleneck). In the ablation study, the protocol agrees with Tab. 1, and the testing set is VIPL [31]. Results in Tab. 6 indicate that a proper projection layer can significantly improve the performance. This is because the projection layer can extract inherent physiological information among different instances while alleviating their differentials. For example, some instances in UBFC [2] is experimentally proven to convey the diastolic peak, while other instances may not have this property. Under this circumstance, a proper projection layer can effectively align these instances, leading to better generalization.

**Figure 6: Ablation study on hyperparameters of DOHA.****Figure 7: Visualization on the effect of DOHA: the relationship among the instances from different attributes becomes smoother [8, 29] (i.e. more uniformed).**

**Discussion on computing resource.** DOHA’s time consumption (training stage) is acceptable due to the lightweight model structure [20, 58] and small batch size (e.g., 4 in [60]) of rPPG network training. Besides, the ablation study in Fig. 6 (c) demonstrates that DOHA can work reliably with different widely-used batch sizes. Furthermore, DOHA’s time consumption during inference is either negligible. We describe these time consumptions in detail in the Appendix. E. **Visualization.** To illustrate the effect of DOHA, we visualize the relationship among the gradients of instances in VIPL and UBFC, with the baseline [20] trained on these databases. Results in Fig. 7 demonstrate that DOHA helps the baseline model find a smoother solution in the parameter hyperplane: (1) The gradients corresponding to similar attributes (highlighted by the blue box) exhibit restricted extreme similarity, indicating that the excessive training towards these attributes, which can lead to overfitting, is mitigated. (2) Conflicts among different attributes (highlighted by the green box) are alleviated, as evidenced by the reduced negative correlation. Such a phenomenon suggests that DOHA promotes a more balanced representation of different attributes.

## 5 CONCLUSION

In this paper, we define and analyze the domain conflict problem in the rPPG task. We then introduce the DOmain-HArmonious framework (DOHA) to alleviate this problem. DOHA consists of two components, one that neutralizes the unknown phase differentials among instances, and another that alleviates the irrelevant attribute conflicts among different training scenarios. By addressing these conflicts, DOHA enables the rPPG model to focus more on the underlying physiological nature present in the instances, leading to improved generalization performance on unseen scenarios. Importantly, DOHA can be easily integrated into existing DL rPPG methods without requiring additional knowledge such as the domain label. We have conducted extensive experiments to evaluate the effect of DOHA.

## ACKNOWLEDGMENTS

This work was supported in part by Jiangsu Provincial Social Development Key R&D Program (BE2020685).



## REFERENCES

- [1] Salma Alhagry, Aly Aly Fahmy, and Reda A El-Khoribi. Emotion recognition based on eeg using lstm recurrent neural network. *International Journal of Advanced Computer Science and Applications*, 8(10), 2017.
- [2] Serge Bobbia, Richard Macwan, Yannick Benezeth, Alamin Mansouri, and Julien Dubois. Unsupervised skin tissue segmentation for remote photoplethysmography. *Pattern Recognition Letters*, 124:82–90, 2019.
- [3] Giuseppe Boccignone, Donatello Conte, Vittorio Cuculo, Alessandro D’Amelio, Giuliano Grossi, and Raffaella Lanzarotti. An open framework for remote-PPG methods and their assessment. *IEEE Access*, pages 1–1, 2020.
- [4] Tiffany Tianhui Cai, Jonathan Frankle, David J Schwab, and Ari S Morcos. Are all negatives created equal in contrastive instance discrimination? *arXiv preprint arXiv:2010.06682*, 2020.
- [5] Weixuan Chen and Daniel McDuff. Deepphys: Video-based physiological measurement using convolutional attention networks. In *ECCV*, 2018.
- [6] Wei-Hao Chung, Cheng-Ju Hsieh, Sheng-Hung Liu, and Chiou-Ting Hsu. Domain generalized rppg network: Disentangled feature learning with domain permutation and domain augmentation. In *Proceedings of the Asian Conference on Computer Vision*, pages 807–823, 2022.
- [7] Gerard De Haan and Vincent Jeanne. Robust pulse rate from chrominance-based rppg. *IEEE Transactions on Biomedical Engineering*, 60(10):2878–2886, 2013.
- [8] Pierre Foret, Ariel Kleiner, Hossein Mobahi, and Behnam Neyshabur. Sharpness-aware minimization for efficiently improving generalization. *CoRR*, abs/2010.01412, 2020.
- [9] Yaroslav Ganin and Victor Lempitsky. Unsupervised domain adaptation by backpropagation. In *International conference on machine learning*, pages 1180–1189. PMLR, 2015.
- [10] Min Hu, Fei Qian, Dong Guo, Xiaohua Wang, Lei He, and Fuji Ren. Eta-rppgnet: Effective time-domain attention network for remote heart rate measurement. *IEEE Transactions on Instrumentation and Measurement*, 70:1–12, 2021.
- [11] Sinh Huynh, Rajesh Krishna Balan, Jeong Gil Ko, and Youngki Lee. Vitamon: Measuring heart rate variability using smartphone front camera. In Mi Zhang, editor, *SenSys 2019 - Proceedings of the 17th Conference on Embedded Networked Sensor Systems*, SenSys 2019 - Proceedings of the 17th Conference on Embedded Networked Sensor Systems, pages 1–14. Association for Computing Machinery, Nov. 2019. Publisher Copyright: © 2019 ACM; 17th ACM Conference on Embedded Networked Sensor Systems, SenSys 2019 ; Conference date: 10-11-2019 Through 13-11-2019.
- [12] Seogkyu Jeon, Kibeom Hong, Pilhyeon Lee, Jewook Lee, and Hyeran Byun. Feature stylization and domain-aware contrastive learning for domain generalization. In *Proceedings of the 29th ACM International Conference on Multimedia*, MM ’21, page 22–31, New York, NY, USA, 2021. Association for Computing Machinery.
- [13] Viktor Kessler, Patrick Thiam, Mohammadreza Amirian, and Friedhelm Schwenker. Pain recognition with camera photoplethysmography. In *2017 Seventh International Conference on Image Processing Theory, Tools and Applications*, pages 1–5. IEEE, 2017.
- [14] Davis E King. Max-margin object detection. *arXiv preprint arXiv:1502.00046*, 2015.
- [15] David Krueger, Ethan Caballero, Joern-Henrik Jacobsen, Amy Zhang, Jonathan Binas, Dinghui Zhang, Remi Le Priol, and Aaron Courville. Out-of-distribution generalization via risk extrapolation (rex). In *International Conference on Machine Learning*, pages 5815–5826. PMLR, 2021.
- [16] Eugene Lee, Evan Chen, and Chen-Yi Lee. Meta-rppg: Remote heart rate estimation using a transductive meta-learner. In *European Conference on Computer Vision*, pages 392–409. Springer, 2020.
- [17] Magdalena Lewandowska, Jacek Rumiński, Tomasz Kocejko, and Jędrzej Nowak. Measuring pulse rate with a webcam – a non-contact method for evaluating cardiac activity. In *2011 Federated Conference on Computer Science and Information Systems*, pages 405–410, 2011.
- [18] Buyu Li, Yu Liu, and Xiaogang Wang. Gradient harmonized single-stage detector. In *Proceedings of the AAAI conference on artificial intelligence*, volume 33, pages 8577–8584, 2019.
- [19] Bofan Lin, Xiaobai Li, Zitong Yu, and Guoying Zhao. Face liveness detection by rppg features and contextual patch-based cnn. In *Proceedings of the 2019 3rd international conference on biometric engineering and applications*, pages 61–68, 2019.
- [20] Xin Liu, Josh Fromm, Shwetak Patel, and Daniel McDuff. Multi-task temporal shift attention networks for on-device contactless vitals measurement. *Advances in Neural Information Processing Systems*, 33:19400–19411, 2020.
- [21] Ilya Loshchilov and Frank Hutter. Sgdr: Stochastic gradient descent with warm restarts. *arXiv preprint arXiv:1608.03983*, 2016.
- [22] Hao Lu, Hu Han, and S Kevin Zhou. Dual-gan: Joint bvp and noise modeling for remote physiological measurement. In *Proceedings of the IEEE/CVF Conference on Computer Vision and Pattern Recognition*, pages 12404–12413, 2021.
- [23] Hao Lu, Zitong Yu, Xuesong Niu, and Yingcong Chen. Neuron structure modeling for generalizable remote physiological measurement, 2023.
- [24] Ewa Magdalena Nowara, Tim K Marks, Hassan Mansour, and Ashok Veeraraghavan. Sparseppg: Towards driver monitoring using camera-based vital signs estimation in near-infrared. In *Proceedings of the IEEE conference on computer vision and pattern recognition workshops*, pages 1272–1281, 2018.
- [25] Lucas Mansilla, Rodrigo Echeveste, Diego H. Milone, and Enzo Ferrante. Domain generalization via gradient surgery, 2021.
- [26] Daniel McDuff. Applications of camera-based physiological measurement beyond healthcare. In *Contactless Vital Signs Monitoring*, pages 165–177. Elsevier, 2022.
- [27] Daniel McDuff. Camera measurement of physiological vital signs. *ACM Computing Surveys*, 55(9):1–40, 2023.
- [28] Jochen Meyer, Anastasia Kazakova, Merlin Büsing, and Susanne Boll. Visualization of complex health data on mobile devices. In *Proceedings of the 2016 ACM Workshop on Multimedia for Personal Health and Health Care*, pages 31–34, 2016.
- [29] Shuaicheng Niu, Jiaxiang Wu, Yifan Zhang, Zhiquan Wen, Yafo Chen, Peilin Zhao, and Mingkui Tan. Towards stable test-time adaptation in dynamic wild world. *arXiv preprint arXiv:2302.12400*, 2023.
- [30] Xuesong Niu, Hu Han, Shiguang Shan, and Xilin Chen. Synrhythm: Learning a deep heart rate estimator from general to specific. In *2018 24th International Conference on Pattern Recognition*, pages 3580–3585, 2018.
- [31] X. Niu, H. Han, S. Shan, and X. Chen. Vipl-hr: A multi-modal database for pulse estimation from less-constrained face video. 2018.
- [32] Xuesong Niu, Shiguang Shan, Hu Han, and Xilin Chen. Rhythmet: End-to-end heart rate estimation from face via spatial-temporal representation. *IEEE Transactions on Image Processing*, 29:2409–2423, 2020.
- [33] Xuesong Niu, Zitong Yu, Hu Han, Xiaobai Li, Shiguang Shan, and Guoying Zhao. Video-based remote physiological measurement via cross-verified feature disentangling. In *European Conference on Computer Vision*, 2020.
- [34] Giambattista Parascandolo, Alexander Neitz, Antonio Orvieto, Luigi Gresele, and Bernhard Schölkopf. Learning explanations that are hard to vary. *arXiv preprint arXiv:2009.00329*, 2020.
- [35] Ming-Zher Poh, Daniel J McDuff, and Rosalind W Picard. Non-contact, automated cardiac pulse measurements using video imaging and blind source separation. *Optics express*, 18(10):10762–10774, 2010.
- [36] Ming-Zher Poh, Daniel J. McDuff, and Rosalind W. Picard. Advancements in noncontact, multiparameter physiological measurements using a webcam. *IEEE Transactions on Biomedical Engineering*, 58(1):7–11, 2011.
- [37] Rita Meziati Sabour, Yannick Benezeth, Pierre De Oliveira, Julien Chappe, and Fan Yang. Ubcf-phys: A multimodal database for psychophysiological studies of social stress. *IEEE Transactions on Affective Computing*, 2021.
- [38] Shiv Shankar, Vihari Piratla, Soumen Chakrabarti, Siddhartha Chaudhuri, Preethi Jyothi, and Sunita Sarawagi. Generalizing across domains via cross-gradient training. *arXiv preprint arXiv:1804.10745*, 2018.
- [39] Robin P Smith, Jérôme Argod, Jean-Louis Pépin, and Patrick A Lévy. Pulse transit time: an appraisal of potential clinical applications. *Thorax*, 54(5):452–457, 1999.
- [40] Rencheng Song, Senle Zhang, Chang Li, Yunfei Zhang, Juan Cheng, and Xun Chen. Heart rate estimation from facial videos using a spatiotemporal representation with convolutional neural networks. *IEEE Transactions on Instrumentation and Measurement*, 69(10):7411–7421, 2020.
- [41] Radim Špetlík, Vojtech Franc, and Jiri Matas. Visual heart rate estimation with convolutional neural network. In *Proceedings of the british machine vision conference*, Newcastle, UK, pages 3–6, 2018.
- [42] Ronny Stricker, Steffen Müller, and Horst-Michael Gross. Non-contact video-based pulse rate measurement on a mobile service robot. In *The 23rd IEEE International Symposium on Robot and Human Interactive Communication*, pages 1056–1062, 2014.
- [43] Bo Sun, Qinglan Wei, Liandong Li, Qihua Xu, Jun He, and Lejun Yu. Lstm for dynamic emotion and group emotion recognition in the wild. In *Proceedings of the 18th ACM international conference on multimodal interaction*, pages 451–457, 2016.
- [44] Zhaodong Sun and Xiaobai Li. Contrast-phys: Unsupervised video-based remote physiological measurement via spatiotemporal contrast. In *European Conference on Computer Vision*, pages 492–510. Springer, 2022.
- [45] Chris Xing Tian, Hao Liang Li, Xiaofei Xie, Yang Liu, and Shiqi Wang. Neuron coverage-guided domain generalization. *IEEE Transactions on Pattern Analysis and Machine Intelligence*, 45(1):1302–1311, 2022.
- [46] Yun-Yun Tsou, Yi-An Lee, Chiou-Ting Hsu, and Shang-Hung Chang. Siamese-rppg network: Remote photoplethysmography signal estimation from face videos. In *Proceedings of the 35th annual ACM symposium on applied computing*, pages 2066–2073, 2020.
- [47] Goran Udovičić, Jurica Derek, Mladen Russo, and Marjan Sikora. Wearable emotion recognition system based on gsr and ppg signals. In *Proceedings of the 2nd international workshop on multimedia for personal health and health care*, pages 53–59, 2017.
- [48] Wim Verkrusse, Lars O Svaasand, and J Stuart Nelson. Remote plethysmographic imaging using ambient light. *Optics express*, 16(26):21434–21445, 2008.
- [49] Jingye Wang, Ruoyi Du, Dongliang Chang, Kongming Liang, and Zhanyu Ma. Domain generalization via frequency-domain-based feature disentanglement and interaction. In *Proceedings of the 30th ACM International Conference on Multimedia*, MM ’22, page 4821–4829, New York, NY, USA, 2022. Association for Computing Machinery.
- [50] Jindong Wang, Cuiling Lan, Chang Liu, Yidong Ouyang, Tao Qin, Wang Lu, Yiqiang Chen, Wenjun Zeng, and Philip Yu. Generalizing to unseen domains: A survey on domain generalization. *IEEE Transactions on Knowledge and Data Engineering*, 2022.

- [51] Mengzhu Wang, Jianlong Yuan, Qi Qian, Zhibin Wang, and Hao Li. Semantic data augmentation based distance metric learning for domain generalization. In *Proceedings of the 30th ACM International Conference on Multimedia*, MM '22, page 3214–3223, New York, NY, USA, 2022. Association for Computing Machinery.
- [52] Wenjin Wang, Albertus C Den Brinker, Sander Stuijk, and Gerard De Haan. Algorithmic principles of remote ppg. *IEEE Transactions on Biomedical Engineering*, 64(7):1479–1491, 2016.
- [53] Hao-Yu Wu, Michael Rubinstein, Eugene Shih, John Guttag, Frédo Durand, and William Freeman. Eulerian video magnification for revealing subtle changes in the world. *ACM transactions on graphics*, 31(4):1–8, 2012.
- [54] Lin Xi, Weihai Chen, Changchen Zhao, Xingming Wu, and Jianhua Wang. Image enhancement for remote photoplethysmography in a low-light environment. In *2020 15th IEEE International Conference on Automatic Face and Gesture Recognition*, pages 1–7. IEEE, 2020.
- [55] Chenglin Yao, Shihe Wang, Jialu Zhang, Wentao He, Heshan Du, Jianfeng Ren, Ruibin Bai, and Jiang Liu. rppg-based spoofing detection for face mask attack using efficientnet on weighted spatial-temporal representation. In *2021 IEEE International Conference on Image Processing*, pages 3872–3876. IEEE, 2021.
- [56] Tianhe Yu, Saurabh Kumar, Abhishek Gupta, Sergey Levine, Karol Hausman, and Chelsea Finn. Gradient surgery for multi-task learning, 2020.
- [57] Zitong Yu, Rizhao Cai, Zhi Li, Wenhao Yang, Jingang Shi, and Alex C Kot. Benchmarking joint face spoofing and forgery detection with visual and physiological cues. *arXiv preprint arXiv:2208.05401*, 2022.
- [58] Zitong Yu, Xiaobai Li, and Guoying Zhao. Remote photoplethysmograph signal measurement from facial videos using spatio-temporal networks. 2019.
- [59] Zitong Yu, Wei Peng, Xiaobai Li, Xiaopeng Hong, and Guoying Zhao. Remote heart rate measurement from highly compressed facial videos: An end-to-end deep learning solution with video enhancement. In *2019 IEEE/CVF International Conference on Computer Vision*, pages 151–160, 2019.
- [60] Zitong Yu, Yuming Shen, Jingang Shi, Hengshuang Zhao, Philip Torr, and Guoying Zhao. Physformer: Facial video-based physiological measurement with temporal difference transformer. *arXiv preprint arXiv:2111.12082*, 2021.
- [61] Matthew D Zeiler. Adadelta: an adaptive learning rate method. *arXiv preprint arXiv:1212.5701*, 2012.

## A DETAILS ON INVOLVED DATABASES

This section demonstrates the details of different external attributes of the involved databases.

(1) **VIPL-HR**. Subjects in VIPL-HR database mainly have yellow skin. Each subject participates in 9 different tasks (namely v1-v9). In our main text, we utilize 6 tasks (i.e. v1-v6) for illustration. The main attributes of these 6 tasks are described as follows:

**v1**. The head movement of the subject is small, and the illumination condition is normal (i.e. as usual).

**v2**. The head movement of the subject is large (e.g., fierce head shaking), and the illumination condition is normal.

**v3**. The head movement of the subject is middle (e.g., speaking), and the illumination condition is normal.

**v4**. The head movement of the subject is small, and the illumination condition is high (i.e. bright).

**v5**. The head movement of the subject is small, and the illumination condition is low (i.e. dark).

**v6**. The head movement of the subject is small, and the illumination condition is normal (i.e. as usual). And the subject sits relatively far (about 2m) in front of other tasks (about 0.5m).

**v7**. The head movement of the subject is small, and the illumination condition is normal (i.e. as usual). And the subject’s heart rate is high as he/she is after outdoor sports.

**v8**. The head movement of the subject is small, and the illumination condition is normal (i.e. as usual). And the subject holds the camera to record facial videos, which may introduce motion because of the head (which holds the camera) movement.

**v9**. The head movement of the subject is large, and the illumination condition is normal (i.e. as usual). And the subject holds the camera to record facial videos, which may introduce motion because of the head (which holds the camera) movement.

(2) **UBFC**. Subjects in UBFC database mainly have white skin. The video numbers in UBFC is far smaller than those in VIPL, adding the average difficulty of the tasks in UBFC is relative low and balanced, we view them as a whole group in the illustration (Fig. 8) in the main text.

(3) **PURE**. Subjects in PURE database mainly have white skin, and the illumination is comparable low. The video numbers in PURE is far smaller than those in VIPL, adding the average difficulty of the tasks in UBFC is relative low and balanced, we view them as a whole group in the illustration (Fig. 5) in the main text.

## B NETWORK ADJUSTMENT

In our experiments, the input size of the facial video is  $[T \times 3 \times 131 \times 131]$ , and we apply this size in all involved end-to-end rPPG networks (i.e., Deepphys, TS-CAN, PhysNet). This input size is different from those in the original settings (e.g., in Deepphys, the input size is  $[T \times 3 \times 36 \times 36]$ ). In this section, we introduce our adjusted TS-CAN (the baseline in Tab. 1), as shown in Fig. 8. Moreover, the detailed implementation of our harmonious phase strategy (under inference) on this adjusted baseline is shown in Fig. 9.

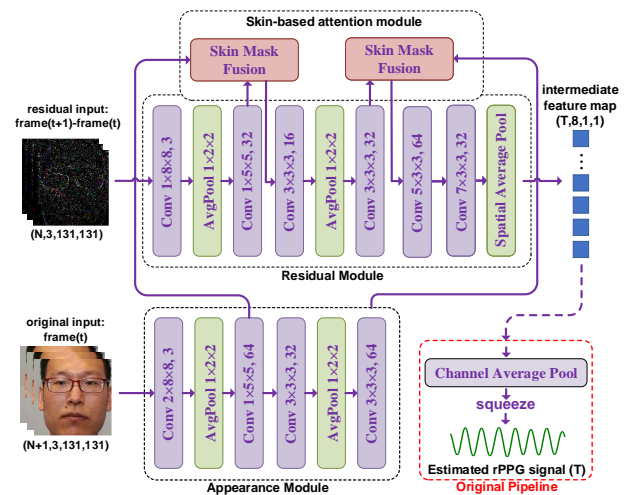


Figure 8: The adjusted baseline (i.e. TS-CAN) in our experiment. The “Skin Mask Fusion” can refer to original paper, which is the same.

## C ALGORITHM FOR SSP MAP GENERATION

In the main text, due to space limitation, we use Fig. 3 to briefly introduce the generation of self-similarity physiological (SSP) map. In this section, we use pseudo code to specifically describe the generation progress, as shown in Algorithm. 3.

## D LIMITATION OF SIGNAL CALIBRATION

The main text mentions that we can utilize traditional rPPG methods (e.g., GREEN) to calibrate the phase differentials among the “ground truth” and actual facial rPPG signals. However, this method is laborious and wasteful. The main problem is that such a standard for calibration is usually hard to acquire: the results in Tab. 1 indicate that these traditional methods cannot perform well under

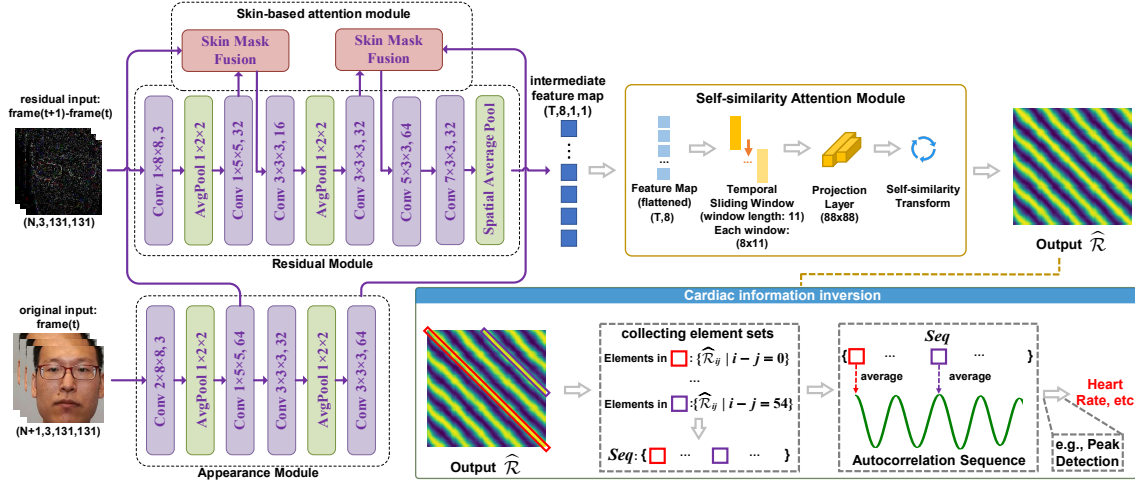


Figure 9: The adjusted baseline combined with proposed DOHA, and we detailed describe the process of “cardiac information inversion” (algorithm 1 in the main text) in the blue box.

### Algorithm 3 Self-similarity physiological map generation

- 1: **Input:** Physiological signal  $Sig : \{t_0, t_1, \dots, t_{N-1}\}$ , length of signal  $N$ , sliding window length  $L_w$ , similarity calculating function  $sim(\cdot, \cdot)$
- 2: Define output map size  $L_o = N - L_{win} + 1$ , initialize slice list  $List_{sl} = [0]_{L_o}$ , initialize self-similarity physiological map  $\mathcal{R}_{L_o \times L_o} = [0]_{L_o \times L_o}$
- 3:  $List_{sl}[i] \leftarrow \{t_i, t_{i+1}, \dots, t_{i+L_{win}-1}\}, \forall i \in [0, L_o - 1]$   
% self-similarity transform %
- 4: **for**  $i \in [0, L_o - 1]$  **do**
- 5:     **for**  $j \in [0, L_o - 1]$  **do**
- 6:          $\mathcal{R}_{ij} \leftarrow sim(List[i], List[j])$
- 7: **Output:** Self-similarity physiological map  $\mathcal{R}_{L_o \times L_o}$

challenging scenarios such as instances in the VIPL-HR database. To verify this, we put the utilization of the database (VIPL-HR, source 2) after calibration, as shown in Fig. 10, from which we can observe that those challenging tasks (e.g., those in v2, v3) all get eliminated throughout the sifting. The decrement in data utilization could damage the diversity of training scenarios, thus impacting the model generalization.

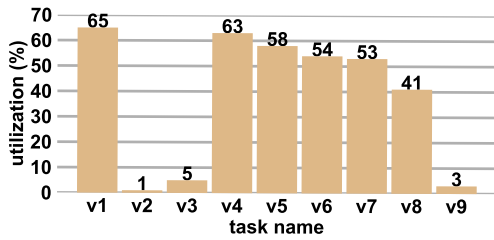


Figure 10: The utilization of VIPL-HR (source2) after calibration via GREEN. We can observe that few instances can be utilized in tasks v2, v3, v8, v9, which are all difficult tasks.

Furthermore, we use the sifted data to present the delay distribution among the “ground truth” and actual facial rPPG signals,

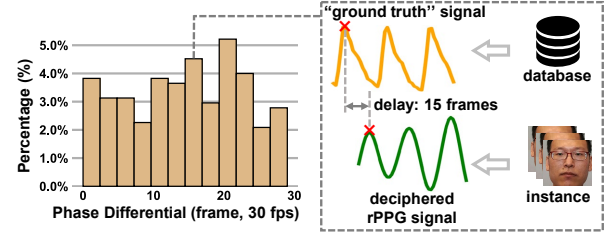


Figure 11: The probability density of phase delays among instances with VIPL database [31] that can be deciphered (i.e., analyzed with high confidence) using GREEN [48].

Table 7: Time consumption of DOHA, when training we use a batch size of 5, and video length is 75. The involved baseline is adjusted TS-CAN. The input frame size is  $131 \times 131$ .

	Training time per batch)	Inference time on 300 frames video
[1pt] Baseline	0.526	0.413
DOHA+ (w/o HPS)	1.764	0.413
DOHA+ (w/o GGH)	1.935	0.607
DOHA+ (w/o IGH)	0.960	0.607
DOHA+	1.934	0.607

as shown in 11. From the results, we can infer that such delay is genuinely uncertain and cannot be neglected (with the max delay about the whole cardiac period).

## E TIME CONSUMPTION OF DOHA

The time consumption of DOHA is listed as Tab. 7. From the table, the primary time consumption is associated with IGH and GGH, as they involve instance-level gradient operations. However, these operations do not affect the time consumption during the inference stage. Conversely, DOHA-HPS also works during inference time but requires lower time consumption.